Idealized glass transitions for a system of dumbbell molecules

S.-H. Chong and W. Götze

Physik Department, Technische Universität München, 85747 Garching, Germany

The mode-coupling theory for ideal glass transitions in simple systems is generalized to a theory for the glassy dynamics of molecular liquids using the density fluctuations of the sites of the molecule's constituent atoms as the basic structure variables. The theory is applied to calculate the liquid-glass phase diagram and the form factors for the arrested structure of a system of symmetric dumbbells of fused hard spheres. The static structure factors, which enter the equations of motion as input, are calculated as function of the packing fraction φ and the molecule's elongation ζ within the reference-interaction-site-model and Percus-Yevick theories. The critical packing fraction φ_c for the glass transition is obtained as nonmonotone function of ζ with a maximum near $\zeta = 0.43$. A transition line is calculated separating a small-ζ-glass phase with ergodic dipole motion from a large-ζ-glass phase where also the reorientational motion is arrested. The Debye-Waller factors at the transition are found to be somewhat larger for sufficiently elongated systems than those for the simple hard-sphere system, but the wave-number dependence of the glass-form factors is quite similar. The dipole reorientations for $\zeta \gtrsim 0.6$ are arrested as strongly as density fluctuations with wave vectors at the position of the first sharp diffraction peak.

I. INTRODUCTION

The mode-coupling theory (MCT) for idealized liquid-glass transitions has been proposed originally as a microscopic approximation theory for the dynamics of simple liquids [1]. The MCT equations formulate the idea that correlation functions for density fluctuations have to be evaluated self-consistently with the correlation functions for force fluctuations. The derived equations require the static structure factor as input, which is anticipated to be a smooth function of the wave vector and of control parameters, such as the packing fraction φ. The equations exhibit a bifurcation singularity for certain values of the control parameters, say, for $\varphi = \varphi_c$. For $\varphi < \varphi_c$, the solutions describe ergodic liquid dynamics, while for $\varphi \geq \varphi_c$ nonergodic dynamics is obtained describing an amorphous solid. The arrested glass structure for $\varphi \geq \varphi_c$ is characterized by glass-form factors, also referred to as nonergodicity parameters. They generalize the concept of the Edwards-Anderson parameter from the theory of spin glasses [2]; they can be determined in scattering experiments and molecular-dynamics-simulation studies. The MCT equations can be solved by asymptotic expansion using, e.g., $|\varphi - \varphi_c|$ as a small parameter [3,4]. The leading order results establish universal results for the glassy dynamics [5]. Anticipating that these universal formulas are valid also for mixtures and for molecular glass-forming systems, extensive tests of the MCT with data from experiments and simulations have been carried out during the past 10 years [6,7]. Due to the invention of improved spectrometers and progress in simulation techniques, the work of testing MCT is still an active field. Let us mention as particularly impressive recent examples the studies with the optical Kerr effect [8,9], the depolarized-light-scattering work for toluene [10], the quantitative tests of the form factors for silica [11], and the scaling-law analysis of simulation data for a polymer model [12]. The indicated tests suggest that MCT deals properly with some essential features of glass-forming systems.

There is a problem in the tests of the universal MCT formulas: the range of validity of these leading-order asymptotic results is not universal. For example, the time interval for the density-fluctuation decay according to von Schweidler's power law depends nontrivially on the wave vector of the fluctuations. Fitting data by a power law for times outside the regime of validity of the asymptotic law may be possible but can yield misleading conclusions [13]. The range of validity of the leading-order result can be determined by calculating the leading corrections or by comparing with the numerical solutions of the full equations of motion [3,4]. But, for such discussions one has to analyze the complete equations of motion, i.e., one needs an understanding of the microscopic details of the system. Thus, there is the necessity to extend the MCT so that models can be analyzed which describe the experimental situation closely. This is the motivation for the present paper where MCT shall be extended to molecular liquids and where this extension shall be exemplified for a hard-dumbbell system.

Extensions of MCT to molecular systems have been studied already, generalizing the concept of a density-fluctuation correlator to the one of infinite matrices of correlation functions formed with tensor-density fluctuations [14–22]. The results calculated for the glass-form factors for a model of water [16,18] and for a liquid of linear molecules [17] could be used to explain simulation data quantitatively. Promising results for anomalous oscillation spectra for a dipolar-hard-sphere system have been calculated [20]. For the model of a dilute solute of linear molecules in a solvent of spherical particles, the MCT equations could be fully solved [21,22]. The solutions were used to demonstrate the applicability of the universal formulas also for reorientational motion and to explain the characteristic difference between the α peaks for dielectric-loss and depolarized-light-scattering spectra, as they have been observed in some experiments for van der Waals liquids. The cited work shows that MCT studies may contribute to the understanding of glassy dynamics, which is

65 041503-1

beyond the implications of universality.

The MCT equations based on the tensor-density description of molecular systems have a different mathematical structure than the ones studied so far. It is unclear whether the bifurcation dynamics of these equations exhibits the same universal laws as derived within the MCT for atomic systems. It is not obvious that codes can be developed for the numerical solutions of these equations within the regime of glassy dynamics. Therefore, it was suggested to base the MCT for molecular systems on the site representation [23–25]. This leads to equations with $n \times n$ matrices where n is the number of atoms producing the force centers in the molecules. For the simple case of a dilute solution of linear molecules, it was shown that this approach yields results [24] in semiquantitative agreement with the much more involved tensor-density theory [22]. In the present paper, this work shall be continued with the intention to demonstrate a complete set of results for the glassy dynamics of a system of linear molecules.

The paper is organized as follows. The basic general MCT equations are obtained in the Appendix by modification and generalization of the previous work [23,24]. They are specialized in Sec. II to a formulation of the equations of motion for the coherent and incoherent density correlation functions for the symmetric-hard-dumbbell system. The static structure factors, which determine the mode-coupling coefficients, are evaluated within the reference-interaction-site-model (RISM) theory. To analyze their features in Sec. III, they are decomposed in their various angular momentum contributions which are evaluated within the Percus-Yevick theory. Section IV explains the phase diagram for the system and the glass-form factors. The conclusions (Sec. V) summarize the results while the discussion of the correlation functions is left for a following paper [26].

II. A MODE-COUPLING THEORY FOR A SYSTEM OF SYMMETRIC DUMBBELLS

A. The model

A system of N rigid dumbbell molecules distributed with density ρ is considered. The molecule shall be described within the interaction-site formalism [27,28], where the constituent atoms shall be called A and B. Let $\vec{r}_i^a$, $a = A$, or B, denote the position vectors of the atoms in the ith molecule, so that $L = |\vec{r}_i^A - \vec{r}_i^B|$ denotes the distance between the two interaction sites. Vector $\vec{e}_i = (\vec{r}_i^A - \vec{r}_i^B)/L$ abbreviates the axis of the ith molecule. Denoting the mass of atom a as m_a, the total mass $M = m_A + m_B$ and the moment of inertia $I = m_A m_B L^2/M$ determine the thermal velocities $v_T = \sqrt{k_B T/M}$ and $v_R = \sqrt{k_B T/I}$ for the molecule's translation and rotation, respectively. Here T denotes the temperature. Let us introduce also the center-of-mass position $\vec{r}_i^C = (m_A \vec{r}_i^A + m_B \vec{r}_i^B)/M$ and the coordinates z_a of the atoms along the molecule's axis: $z_A = L(m_B/M)$, $z_B = -L(m_A/M)$. The basic structural variables are the two interaction-site-density fluctuations for wave vectors $\vec{q}$

$$\rho_q^a = \sum_{i=1}^{N} \exp(i\vec{q} \cdot \vec{r}_i^a), \quad a = A \quad \text{or} \quad B. \quad (1)$$

The site-site static structure factors $S_q^{ab} = \langle \rho_q^{a*} \rho_q^b \rangle / N$ provide the simplest information on the equilibrium structure of the system. Here $\langle \cdots \rangle$ denotes canonical averaging. Because of isotropy, S_q^{ab} depends only on the wave number $q = |\vec{q}|$. The site-site static structure factor S_q^{ab} consists of the intramolecular and intermolecular parts. The former is denoted as w_q^{ab}; for a rigid dumbbell molecule it is given by $w_q^{ab} = \delta^{ab} + (1 - \delta^{ab}) j_0(qL)$. Here and in the following $j_\ell(x)$ denotes the spherical Bessel function of index ℓ. The static structure factors S_q^{ab} shall be combined to a 2×2 matrix $\mathbf{S}_q$, and similar matrix notation will be used for other site-site correlation functions. The site-site Ornstein-Zernike equation [27,28], $\mathbf{S}_q = [\mathbf{w}_q^{-1} - \rho \mathbf{c}_q]^{-1}$, relates S_q^{ab} to the site-site direct correlation function c_q^{ab}.

The structural dynamics of the system shall be described by the interaction-site-density correlators

$$F_q^{ab}(t) = \langle \rho_q^a(t)^* \rho_q^b(0) \rangle / N. \quad (2)$$

These are real even functions of time obeying $F_q^{ab}(t) = F_q^{ba}(t)$. The short-time expansion can be written as

$$\mathbf{F}_q(t) = \mathbf{S}_q - \frac{1}{2} q^2 \mathbf{J}_q t^2 + O(t^4). \quad (3)$$

The continuity equation reads $\dot{\rho}_q^a = i\vec{q} \cdot \vec{j}_q^a$, where the longitudinal current fluctuation is given by $\vec{j}_q^a = \Sigma_i \vec{v}_i^a \exp(i\vec{q} \cdot \vec{r}_i^a)$ with $\vec{v}_i^a$ denoting the velocity of atom a in the ith molecule. Therefore, one gets $J_q^{ab} = \langle (\vec{q} \cdot \vec{j}_q^a)^* (\vec{q} \cdot \vec{j}_q^b) \rangle / Nq^2$, whose explicit expressions for a rigid dumbbell molecule are given by [29]

$$J_q^{ab} = v_T^2 w_q^{ab} + v_R^2 \left(\frac{2}{3} z_a z_b \right) [\delta^{ab} + (1 - \delta^{ab})$$

$$\times \{ j_0(qL) + j_2(qL) \}]. \quad (4)$$

The dynamics of the tagged molecule shall also be considered. It is described by the self part of the interaction-site-density correlators

$$F_{q,s}^{ab}(t) = \langle \rho_{q,s}^a(t)^* \rho_{q,s}^b(0) \rangle. \quad (5)$$

Here $\rho_{q,s}^a = \exp(i\vec{q} \cdot \vec{r}_s^a)$ with $\vec{r}_s^a$ denoting the position vector of atom a in the tagged molecule. The short-time expansion of the correlator $\mathbf{F}_{q,s}(t)$ is given by Eq. (3) with $\mathbf{S}_q$ replaced by $\mathbf{w}_q$. The same function J_q^{ab} determines the short-time dynamics of $F_{q,s}^{ab}(t)$ since the velocities of different molecules at the same time are statistically independent.

For later convenience, it shall be shown here how the correlation functions in the interaction-site representation can be expressed in terms of the ones in the tensor-density description. Following the convention in Refs. [21] and [22],

coherent tensor-density fluctuations $\rho_\ell^m(\vec{q})$ for the angular-momentum index ℓ and the helicity index m shall be defined by decomposing the ith molecule's position variable in plane waves $\exp(i\vec{q}\cdot\vec{r}_i^C)$ for the center of mass $\vec{r}_i^C$ and in spherical harmonics $Y_\ell^m(\vec{e}_i)$ for the orientation vector $\vec{e}_i$,

$$\rho_\ell^m(\vec{q})=i^\ell\sqrt{4\pi}\sum_{i=1}^N \exp(i\vec{q}\cdot\vec{r}_i^C)Y_\ell^m(\vec{e}_i). \qquad (6)$$

The structural dynamics is described by the matrix of correlators

$$\Phi_{\ell\ell'}^m(q,t)=\langle\rho_\ell^m(\vec{q}_0,t)^*\rho_{\ell'}^m(\vec{q}_0,0)\rangle/N; \quad \vec{q}_0=(0,0,q). \qquad (7)$$

The general correlators $\langle\rho_\ell^m(\vec{q},t)^*\rho_{\ell'}^{m'}(\vec{q},0)\rangle$ can be written as linear combination of the functions $\Phi_{\ell\ell'}^m(q,t)$; they vanish for $m\neq m'$ if $\vec{q}=\vec{q}_0$ [21]. In particular, the equilibrium structure is described by the static correlation functions

$$S_{\ell\ell'}^m(q)=\langle\rho_\ell^m(\vec{q}_0)^*\rho_{\ell'}^m(\vec{q}_0)\rangle/N. \qquad (8)$$

Since the position vectors of the interaction sites can be written as $\vec{r}_i^a=\vec{r}_i^C+z_a\vec{e}_i$, the Rayleigh expansion of the exponential in Eq. (1) yields the formula

$$\rho_{\vec{q}_0}^a=\sum_\ell \sqrt{2\ell+1}j_\ell(qz_a)\rho_\ell^0(\vec{q}_0). \qquad (9)$$

Substitution of this expression into Eq. (2) leads to an expression for the density correlators in the site representation in terms of those in the tensor-density description

$$F_q^{ab}(t)=\sum_{\ell,\ell'} \sqrt{(2\ell+1)(2\ell'+1)}j_\ell(qz_a)j_{\ell'}(qz_b)$$
$$\times\Phi_{\ell\ell'}^0(q,t). \qquad (10)$$

In particular, the site-site static structure factors S_q^{ab} are related to the tensorial ones via

$$S_q^{ab}=\sum_{\ell,\ell'} \sqrt{(2\ell+1)(2\ell'+1)}j_\ell(qz_a)j_{\ell'}(qz_b)S_{\ell\ell'}^0(q). \qquad (11)$$

Similarly, one obtains formulas relating tagged-molecule correlators in the site representation and those in the tensor-density description

$$F_{q,s}^{ab}(t)=\sum_{\ell,\ell'} \sqrt{(2\ell+1)(2\ell'+1)}j_\ell(qz_a)j_{\ell'}(qz_b)$$
$$\times\Phi_{s,\ell\ell'}^0(q,t), \qquad (12)$$

where $\Phi_{s,\ell\ell'}^0(q,t)$ denotes the self part of $\Phi_{\ell\ell'}^0(q,t)$. Since $\Phi_{s,\ell\ell'}^0(q,0)=\delta_{\ell\ell'}$, one gets

$$w_q^{ab}=\sum_\ell (2\ell+1)j_\ell(qz_a)j_\ell(qz_b). \qquad (13)$$

In the present paper, a system of symmetric dumbbell molecules, consisting of two fused hard spheres of diameters $d_A=d_B=d$ and masses $m_A=m_B=M/2$, shall be considered. The elongation parameter $\zeta=L/d$ quantifies the bond length. All equilibrium properties of such a hard-dumbbell system with a fixed elongation are specified by the packing fraction

$$\varphi=\rho V_0, \quad V_0=\frac{\pi}{6}d^3\left(1+\frac{3}{2}\zeta-\frac{1}{2}\zeta^3\right). \qquad (14)$$

Here V_0 is the volume of a dumbbell molecule. Throughout the rest of this paper, the diameter of the constituent atom is chosen as the unit of length $d=1$.

For a symmetric system, there are only two independent density correlators, since $F_q^{AA}(t)=F_q^{BB}(t)$. It is convenient to perform an orthogonal transformation to fluctuations of total number density ρ_q^N and "charge" density ρ_q^Z,

$$\rho_q^x=(\rho_q^A\pm\rho_q^B)/\sqrt{2}, \quad x=N \quad \text{or} \quad Z. \qquad (15a)$$

The transformation matrix $\mathbf{P}=\mathbf{P}^{-1}$ reads

$$\mathbf{P}=\frac{1}{\sqrt{2}}\begin{pmatrix} 1 & 1 \\ 1 & -1 \end{pmatrix}. \qquad (15b)$$

It diagonalizes the matrices $\mathbf{S}_q$, $\mathbf{w}_q$, and $\mathbf{J}_q$ as

$$(\mathbf{PS}_q\mathbf{P})^{xy}=\delta^{xy}S_q^x, \quad S_q^x=S_q^{AA}\pm S_q^{AB}, \qquad (15c)$$

$$(\mathbf{Pw}_q\mathbf{P})^{xy}=\delta^{xy}w_q^x, \quad w_q^x=1\pm j_0(q\zeta), \qquad (15d)$$

$$(\mathbf{PJ}_q\mathbf{P})^{xy}=\delta^{xy}\left(v_T^2 w_q^x+\frac{1}{6}v_R^2\zeta^2[1\mp\{j_0(q\zeta)+j_2(q\zeta)\}]\right), \qquad (15e)$$

where $x,y=N$ or Z. Also the matrix of density correlators is diagonalized. Introducing the density correlators $\phi_q^x(t)$ normalized to $\phi_q^x(t=0)=1$, one gets

$$\phi_q^x(t)=\langle\rho_q^x(t)^*\rho_q^x(0)\rangle/NS_q^x, \quad [\mathbf{PF}_q(t)\mathbf{P}]^{xy}=\delta^{xy}\phi_q^x(t)S_q^x, \qquad (16)$$

and similar equations hold for the normalized tagged-molecule correlators $\phi_{q,s}^x(t)$,

$$\phi_{q,s}^x(t)=\langle\rho_{q,s}^x(t)^*\rho_{q,s}^x(0)\rangle/w_q^x,$$

$$[\mathbf{PF}_{q,s}(t)\mathbf{P}]^{xy}=\delta^{xy}\phi_{q,s}^x(t)w_q^x. \qquad (17)$$

There is an additional property due to the symmetry of the molecule. Since the intermolecular parts of S_q^{AA} and S_q^{AB} are the same, one gets $S_q^Z=w_q^Z$. A similar reasoning for the charge-density correlators leads to

$$\phi_q^Z(t)=\phi_{q,s}^Z(t). \qquad (18)$$

For a system of symmetric dumbbell molecules, there is only one independent coherent density correlator, viz. $\phi_q^N(t)$.

B. MCT equations for the density correlators

The MCT equations of motion for the density correlators consist of an exact Zwanzig-Mori equation and the approximate expression for the relaxation kernel in terms of the mode-coupling functional, whose derivation is described in the Appendix. For a system of symmetric dumbbells, these equations can be simplified considerably [24]. Multiplying Eqs. (A3)–(A7) from left and right with **P** given by Eq. (15b) and inserting $\mathbf{1} = \mathbf{PP}$ between every pair of matrices, all equations are transformed to diagonal ones. Thus, there are two sets of equations, one for $\phi_q^N(t)$ and another for $\phi_q^Z(t)$. As explained in connection with Eq. (18), the charge-density correlator $\phi_q^Z(t)$ is identical to its self part, $\phi_{q,s}^Z(t)$, which shall be treated separately below. Thus, the only correlator describing the coherent density fluctuations is the total density correlator $\phi_q^N(t)$, whose Zwanzig-Mori equation reads

$$\partial_t^2 \phi_q^N(t) + (\Omega_q^N)^2 \phi_q^N(t) + (\Omega_q^N)^2 \int_0^t dt' \, m_q^N(t-t') \partial_{t'} \phi_q^N(t')$$

$$= 0. \qquad (19a)$$

The characteristic frequency Ω_q^N, which specifies the initial decay of the correlator by $\phi_q^N(t) = 1 - \frac{1}{2}(\Omega_q^N t)^2 + O(t^4)$, is given by

$$(\Omega_q^N)^2 = q^2 \left\{ v_T^2[1 + j_0(q\zeta)] \right.$$

$$\left. + \frac{1}{6} v_R^2 \zeta^2 [1 - j_0(q\zeta) - j_2(q\zeta)] \right\} \Big/ S_q^N. \qquad (19b)$$

The relaxation kernel reads $m_q^N(t) = \mathcal{F}_q^N[\phi^N(t)]$, where Eqs. (A5)–(A7) lead to

$$\mathcal{F}_q^N[\tilde{f}] = \frac{1}{2} \int d\vec{k} \, V^N(\vec{q};\vec{k},\vec{p}) \tilde{f}_k \tilde{f}_p, \qquad (20a)$$

$$V^N(\vec{q};\vec{k},\vec{p}) = \frac{\rho}{16\pi^3} S_q^N S_k^N S_p^N \{\vec{q} \cdot [\vec{k} c_k^N + \vec{p} c_p^N]/q^2\}^2, \qquad (20b)$$

with $\vec{p} = \vec{q} - \vec{k}$ and $c_q^N = 2c_q^{AA}$. One gets from Eq. (A11) for the nonergodicity parameters $f_q^N = \phi_q^N(t \to \infty)$,

$$f_q^N = \mathcal{F}_q^N[f^N]/\{1 + \mathcal{F}_q^N[f^N]\}. \qquad (21)$$

Notice that Eqs. (19a), (20), and (21) are formally identical to the corresponding equations for simple systems [3]: the difference is in the definition of the correlators and the direct correlation functions. In particular, one can show that the preceding Eqs. (19)–(21) reduce to the ones for simple systems in both the $\zeta \to 0$ and $\zeta \to \infty$ limits.

The MCT model for the hard-dumbbell system (HDS) will be defined by two further technical assumptions. First, the site-site structure factors S_q^{ab} and the direct correlation
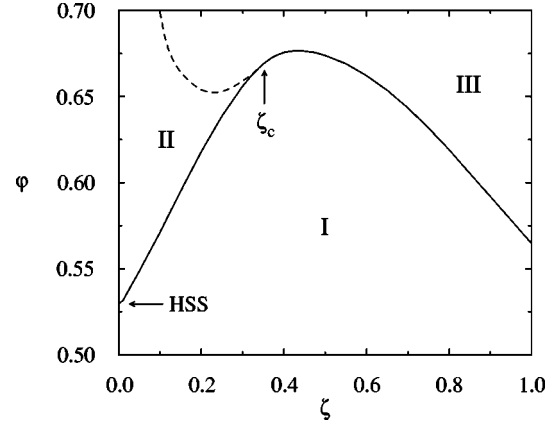

FIG. 1. Phase diagram of the symmetric-hard-dumbbell system where the packing fraction is denoted by φ and the elongation parameter by ζ. The solid curve marks the type-B liquid-glass transition line, $\varphi_c = \varphi_c(\zeta)$. The dashed curve denotes the type-A transition line between phases II and III, $\varphi_A = \varphi_A(\zeta)$. The type-$A$ transition line terminates at the critical elongation $\zeta_c = 0.345$ marked by an arrow. The horizontal arrow marks the transition point of the hard-sphere system (HSS).

functions c_q^{ab} are evaluated within the RISM integral-equation theory [27,28,30]. Second, the wave numbers are discretized to 100 equally spaced values $q = 0.2, 0.6, 1.0, \ldots, 39.8$. The details of the transformation of the mode-coupling functional to a polynomial in the discretized variables can be found in Ref. [3].

The discussion of Eq. (21) can follow that considered previously for simple systems [3]. For a given ζ, one finds a critical packing fraction $\varphi_c = \varphi_c(\zeta)$ so that $f_q^N = 0$ for $\varphi < \varphi_c$ and $f_q^N > 0$ for $\varphi \geq \varphi_c$. Figure 1 exhibits the control-parameter plane for our system; the full line represents the φ_c versus ζ curve. The regime I, i.e., the states with (ζ,φ) below the full line, are the liquid states. For states on and above the line, the density-fluctuation dynamics is nonergodic. It is the purpose of this paper to explain the origin of this liquid-glass-transition curve and to quantify the arrested glass structure.

Comments on some technical details of our calculations are in order. We solved a set of equations in the RISM theory to obtain S_q^{ab} using the nonequally spaced wave-number grids introduced in Ref. [31]. The resulting S_q^{ab} has been subsequently transformed to the one on the above-mentioned equispaced grids using a cubic spline interpolation [32]. Our results for the HDS are based on the S_q^{ab} so obtained. Occasionally, we will refer to results for the hard-sphere system (HSS), i.e., the HDS with $\zeta = 0$. For consistency, calculations for the HSS have also been done using a static structure factor, which is based on the numerical method just mentioned. However, the numerically obtained structure factor for the HSS is, due to the interpolation procedure, slightly different from that of the analytic Percus-Yevick theory [28]. Since the transition is sensitively dependent on the structure-factor peak, this leads to slightly different results for the HSS from the previous ones reported in Ref. [3], where the analytic Percus-Yevick theory is used. Typically, the differences

are less than 1%. Therefore, the results for the HSS based on the two different static inputs can be regarded as essentially the same. The nonstandard wave-number grids from Ref. [31] and the subsequent interpolation procedure have been adopted because of the following reason. The present model shall be extended to one where the constituent atoms carry opposite electrical charges. Thereby it will be possible to study the interplay of steric-hindrance effects and Coulomb-interaction effects. The method developed in Ref. [31] is well suited for treating such a system in which both the short- and long-ranged interactions are simultaneously present. To have the results for the HDS as reference model, it seems adequate to carry out the calculation of the static input function strictly within the same frame.

C. MCT equations for the tagged-molecule correlators

One gets the Zwanzig-Mori equation for the normalized tagged-molecule correlator $\phi_{q,s}^x(t)(x=N$ or $Z)$ for a symmetric-hard-dumbbell system by transforming Eq. (A8) as explained above for deriving Eq. (19a),

$$\partial_t^2 \phi_{q,s}^x(t) + (\Omega_{q,s}^x)^2 \phi_{q,s}^x(t)$$

$$+ (\Omega_{q,s}^x)^2 \int_0^t dt' m_{q,s}^x(t-t') \partial_{t'} \phi_{q,s}^x(t') = 0, \quad x=N \text{ or } Z.$$

$$(22a)$$

The characteristic frequency $\Omega_{q,s}^x$ specifies the initial decay of the correlator by $\phi_{q,s}^x(t) = 1 - \frac{1}{2}(\Omega_{q,s}^x t)^2 + O(t^4)$, and it is given by

$$(\Omega_{q,s}^x)^2 = q^2 \left\{ v_T^2 + \frac{1}{6} v_R^2 \zeta^2 [1 \mp j_0(q\zeta) \right.$$

$$\left. \mp j_2(q\zeta)]/[1 \pm j_0(q\zeta)] \right\}. \quad (22b)$$

The relaxation kernel can be written as $m_{q,s}^x(t) = \mathcal{F}_q^x[\phi_s^x(t), \phi^N(t)]$, where Eqs. (A9) and (A10) lead to

$$\mathcal{F}_{q,s}^x[\tilde{f}_s^x, \tilde{f}] = \frac{\rho}{16\pi^3} \frac{w_q^x}{q^2} \int d\vec{k} \left(\frac{\vec{q} \cdot \vec{p}}{q} \right)^2 (c_p^N)^2 w_k^x S_p^N \tilde{f}_{k,s}^x \tilde{f}_p ,$$

$$(23)$$

with $\vec{p} = \vec{q} - \vec{k}$. From the long time limits of Eqs. (A8) and (A9), one gets for the nonergodicity parameters $f_{q,s}^x = \phi_{q,s}^x(t \to \infty)$,

$$f_{q,s}^x = \mathcal{F}_{q,s}^x[f_s^x, f^N]/\{1 + \mathcal{F}_{q,s}^x[f_s^x, f^N]\}. \quad (24)$$

The mathematical structure of the two sets of Eqs. (22)–(24) for $x=N$ and Z is the same as that studied previously for the tagged-particle-density correlator in a simple liquid [4]. In particular, the set of equations for $x=N$ reduce to that for the tagged-particle-density correlator in both the $\zeta \to 0$ and $\zeta \to \infty$ limits. In the same limits, the correlator $\phi_{q,s}^Z(t)$ becomes identically zero.

Equations (22)–(24) for the tagged symmetric dumbbell immersed in a liquid of symmetric dumbbells are also formally identical to those treated in Refs. [24,25] for the symmetric-dumbbell molecule dissolved in a simple liquid. This is because the coherent density fluctuations of the surroundings in the former case is characterized only by the correlator $\phi_q^N(t)$, i.e., a scalar correlator, and this feature is shared with the latter case. In analogy to the findings in the previous studies, one finds a line of transition points $\varphi_A = \varphi_A(\zeta)$, provided $\zeta \leq \zeta_c = 0.345$. This line, which is shown dashed in Fig. 1, separates glass states in regime II and regime III. In regime II, the reorientational motion is ergodic, i.e., the states deal with the amorphous analog of a plastic crystal. In regime III also the reorientational motion is nonergodic since $f_{q,s}^Z > 0$. Crossing the dashed line by, e.g., increasing φ, $f_{q,s}^Z$ change continuously (type-A transition). Crossing the heavy line, f_q^N changes discontinuously (type-B transition). The interest of the present studies concerns the transition from the liquid to a glass with all density correlators arrested, as obtained for $\zeta > \zeta_c$ by increasing φ. As a representative situation with strong steric hindrance for reorientational motion, molecules with $\zeta = 1.0$ shall be analyzed in detail. For ζ approaching ζ_c from above, the steric hindrance for reorientations weakens, and molecules with $\zeta = 0.4$ shall be used to demonstrate this case.

III. STRUCTURE OF THE RELAXED SYSTEM

The static structure factor for the total density fluctuations S_q^N is the basic input of our theory. It quantifies the simplest information on the averaged particle distribution, anticipating the system to be relaxed in a canonical equilibrium state. The latter is assumed to be an amorphous one. It may be metastable, e.g., with respect to crystallization. The variation of S_q^N with changes of the packing fraction φ and the molecule's elongation ζ provides the key for explaining the phase diagram in Fig. 1. Extending earlier work [33] to the high-density regime, S_q^N shall be analyzed in this section.

A. Static structure factors and angular correlations

Figure 2 exhibits results for S_q^N calculated from the RISM theory [27,28,30] for the two representative elongations $\zeta = 0.4$ and 1.0 at and near the critical packing fraction $\varphi_c(\zeta)$. For small q, the structure factor is small. Because of the dense packing, the compressibility $\kappa_q \propto S_q^N$ for long-wavelength fluctuations is strongly suppressed. These fluctuations are irrelevant for the glassy arrest in our system. The phase diagram does not change more than 1% if fluctuations with, say, $q \lesssim 3$ are cut off. Fluctuations with, say, $q \gtrsim 10$ are relevant, since $S_q^N - 1$ is of order unity. But in this regime, the structure factor is not very sensitive with respect to changes of density. Therefore, the liquid-glass transition is driven mainly by the changes of S_q^N for $q \approx 7$, i.e., by the fluctuations with wave vectors near the position of the first sharp diffraction peak. This feature is analogous to that found in the hard-sphere system [1]. However, the results shown in Fig. 2 are for molecular systems in which angular
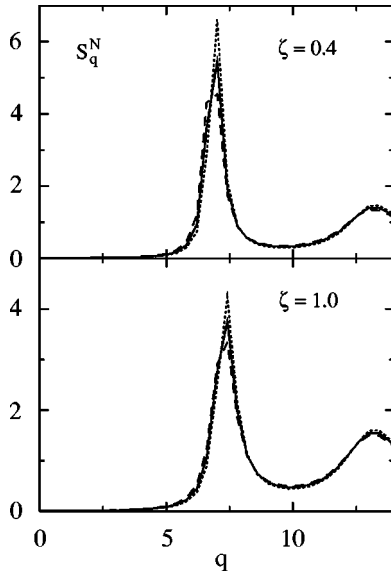
FIG. 2. Static structure factor S_q^N for the total density fluctuations as function of wave number q for the elongations $\zeta = 0.4$ (upper panel) and 1.0 (lower panel). The results refer to packing fractions $\varphi = \varphi_c (1 + \epsilon)$ with $\epsilon = 0$ (solid lines), $\epsilon = -10^{-5/3}$ (dashed lines), and $\epsilon = +10^{-5/3}$ (dotted lines). Here φ_c denotes the critical packing fraction; it is given by $\varphi_c = 0.675$ and 0.565 for $\zeta = 0.4$ and 1.0, respectively. The first sharp diffraction peak in S_q^N for $\zeta = 0.4$ occurs at $q = 7.0$ in the discretized wave-number grids, and its heights are 4.54, 5.47, and 6.61 with increasing φ. The corresponding peak for $\zeta = 1.0$ occurs at $q = 7.4$, and its heights are 3.33, 3.75, and 4.24 with increasing φ. Here and in the following figures the diameter of the spheres is used as unit of length, $d = 1$.

correlations should play an important role as well. This section is devoted to discuss how angular correlations manifest themselves in S_q^N.

To proceed, let us decompose the S_q^N in terms of the spherical-harmonic expansion coefficients $S_{\ell\ell'}^m(q)$ defined in Eq. (8): the coefficient $S_{00}^0(q)$ describes the static center-of-mass density fluctuations, and the higher coefficients probe the angular correlations. This decomposition can be derived from Eq. (11) by noticing the definition $S_q^N = S_q^{AA} + S_q^{AB}$,

$$S_q^N = \sum_{\ell,\ell':even} 2\sqrt{(2\ell+1)(2\ell'+1)} j_\ell(q\zeta/2)$$
$$\times j_{\ell'}(q\zeta/2) S_{\ell\ell'}^0(q). \qquad (25)$$

Here the angular momentum indices ℓ and ℓ' take only even numbers due to the top-down symmetry of the dumbbell molecule. It is clear that the coefficients $S_{\ell\ell'}^0(q)$ contain more information than S_q^N since the latter can be expressed in terms of the former, but not vice versa.

The expansion coefficients $S_{\ell\ell'}^m(q)$ have been calculated within the Percus-Yevick (PY) theory [34,35] up to the angular-momentum-index cutoff $\ell_{cut} = 6$. For the symmetric dumbbell, this results in 30 independent coefficients to be dealt with in solving the PY equation. The representative
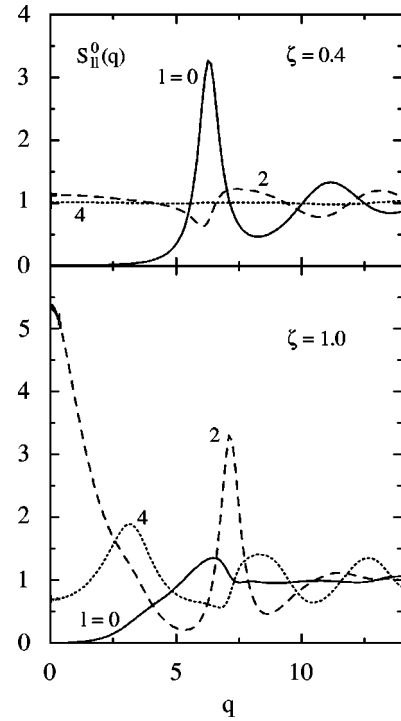

FIG. 3. Spherical-harmonic expansion coefficients $S_{\ell\ell'}^0(q)$ of the structure factor for the elongations $\zeta = 0.4$ (upper panel) and 1.0 (lower panel) at the critical packing fraction $\varphi = \varphi_c$ for the angular momentum indices $\ell = 0$, 2, and 4.

results at the critical packing fraction for the diagonal coefficients $S_{\ell\ell'}^0(q)$ are shown in Fig. 3. For the small elongation $\zeta = 0.4$, the density fluctuations for $q \approx 7$ are dominated by those of the center-of-mass degrees of freedom, $\ell = 0$, while contributions from the reorientational correlations are rather small. On the other hand, for the large elongation $\zeta = 1.0$, the static structure for $q \approx 7$ is primarily caused by the reorientational function $S_{22}^0(q)$, while the center-of-mass component $S_{00}^0(q)$ only shows a weak structure. A strong peak at $q \approx 0$ is also seen in the coefficient $S_{22}^0(q)$ for $\zeta = 1.0$, which is a precursor of a nematic instability. The increased importance of the higher coefficients for larger elongations is demonstrated even more clearly by comparing $S_{44}^0(q)$ for the two elongations. These features of the coefficients $S_{\ell\ell'}^0(q)$ for small and large elongations are in accord with those found in Ref. [36], albeit for fluids of hard ellipsoids in which the aspect ratio plays a role similar to $(1 + \zeta)$.

Figure 4 exhibits the decomposition of S_q^N at the critical packing fraction based on Eq. (25). The solid lines denote S_q^N calculated from the RISM theory, and the dashed and dotted lines denote the terms in the decomposition using the coefficients $S_{\ell\ell'}^0(q)$ from the PY theory. Cross terms ($\ell \neq \ell'$) are omitted to avoid overcrowding of the figures. The function S_q^N from the RISM theory and that based on Eq. (25) with the coefficients $S_{\ell\ell'}^0(q)$ from the PY theory are found to be in good agreement with each other, and therefore it makes sense to discuss the decomposition of S_q^N using the results from two different integral-equation theories. As mentioned in connection with Fig. 2, the glass transition of our
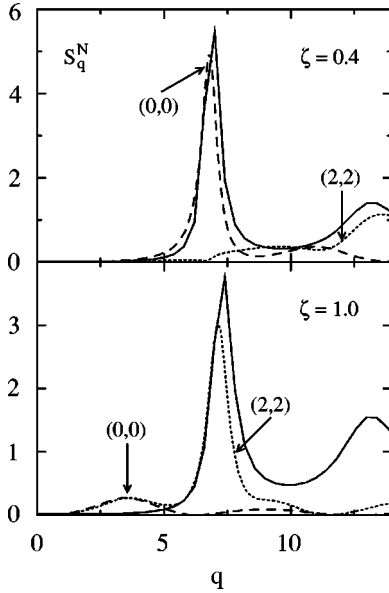
FIG. 4. The solid lines denote the static structure factor S_q^N for the total density fluctuations for the elongation $\zeta = 0.4$ (upper panel) and $\zeta = 1.0$ (lower panel) at the critical packing fraction $\varphi = \varphi_c(\zeta)$. The dashed and dotted lines are the results of decomposition based on Eq. (25), where the numbers in parentheses (ℓ, ℓ) indicate the component in the decomposition (see text).

system is driven by the first peak in S_q^N centered at $q \approx 7$. Figure 4 shows that, for the small elongation, the first peak is primarily determined by the center-of-mass density fluctuations, whilst the contributions from higher-order angular correlations are responsible only for the peaks located in the higher-q region. On the other hand, when the elongation is large, the contribution from the center-of-mass degrees of freedom gets suppressed, but the higher-order angular correlations become much more important for determining the first peak: the first peak is primarily accounted for by the (2,2) contribution. Thus, the static density fluctuations determining the cage for the glass transition are of different origins for small and large elongations, respectively.

A comment shall be added concerning the strong peak in $S_{22}^0(q)$ at $q \approx 0$ shown in Fig. 3 for $\zeta = 1.0$. It is clear from Eq. (25) that the function $S_{22}^0(q)$ contributes to S_q^N with a prefactor $j_2(q\zeta/2)^2$, which is proportional to q^4 for small q. As a result, this strong peak in $S_{22}^0(q)$ hardly contributes to S_q^N in the small wave-number regime; it only gives rise to a small peak centered at $q \approx 3.5$ as shown in Fig. 4. Also, it is seen that the (0,0) component has a peak at the same q range. However, it is found that the small peak at $q \approx 3.5$ is canceled out by the (0,2) component, which is not shown in the figure. All this together results in the small and flat S_q^N for $q < 5$. We conclude that the strong peak in $S_{22}^0(q)$ at $q \approx 0$ is irrelevant for the glass formation for the elongation $\zeta = 1.0$ within our theory.

The intramolecular correlation functions w_q^x $(x = N, Z)$ from Eq. (15d) enter the mode-coupling vertices implicitly via the site-site Ornstein-Zernike equation for $\mathbf{S}_q$ and explicitly via Eq. (23). Using Eq. (13), they can be decomposed in analogy to Eq. (25),
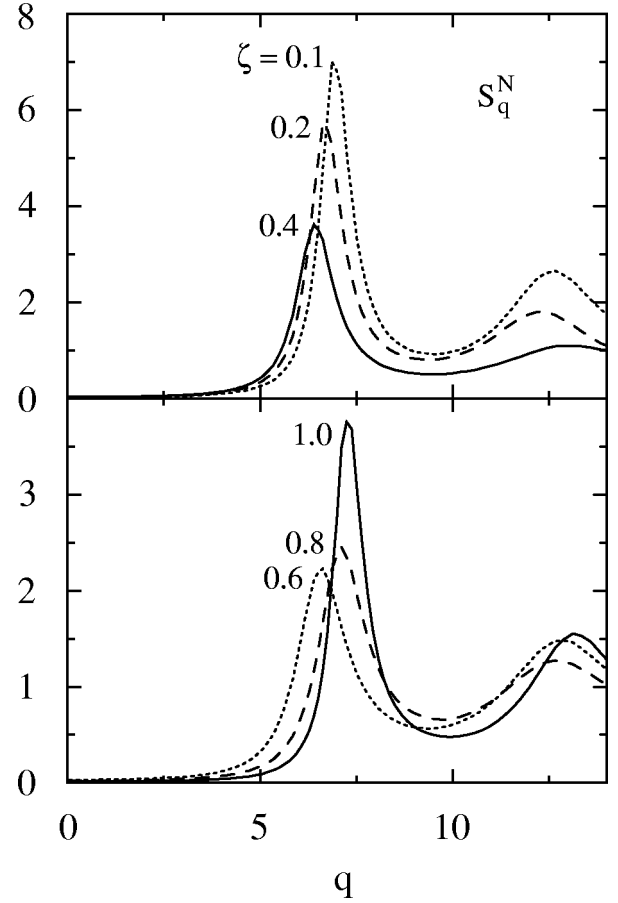

FIG. 5. Static structure factors S_q^N for the total density fluctuations at the fixed packing fraction $\varphi = 0.56$ for various elongations as indicated in the figure.

$$w_q^{N(Z)} = \sum_{\ell : \text{even (odd)}} 2(2\ell+1) j_\ell(q\zeta/2)^2. \quad (26)$$

$w_q^{N(Z)}$ starts for $q = 0$ at the value 2 (0) and then it oscillates for $q > 5$ around the value 1. The first oscillation minima of w_q^N occur at $q = 11.4$ and 27.4 for $\zeta = 0.4$, and at $q = 4.5$ and 11.0 for $\zeta = 1.0$. For w_q^Z, the first minima are located at $q = 19.4$ and 35.0 for $\zeta = 0.4$, and at $q = 7.8$ and 14.2 for $\zeta = 1.0$.

Let us consider the change of the structure factor as a function of the elongation ζ for fixed packing fraction φ. Figure 5 exhibits the result for $\varphi = 0.56$. It is seen that for small elongations (the upper panel) the first peak height decreases with increasing the elongation, whilst the opposite trend is seen for large elongations (the lower panel). This feature can be explained in terms of the spherical-harmonic expansion coefficients $S_{\ell\ell}^0(q)$ as follows. As discussed in connection with Fig. 4, the center-of-mass density fluctuations ($\ell = 0$) are primarily responsible for determining the first peak in S_q^N for small elongations, whereas the angular correlations of the index $\ell = 2$ are more relevant for large elongations. The strength of the center-of-mass correlation becomes weaker as the elongation is increased, and this explains the decrease of the first peak height in S_q^N for small
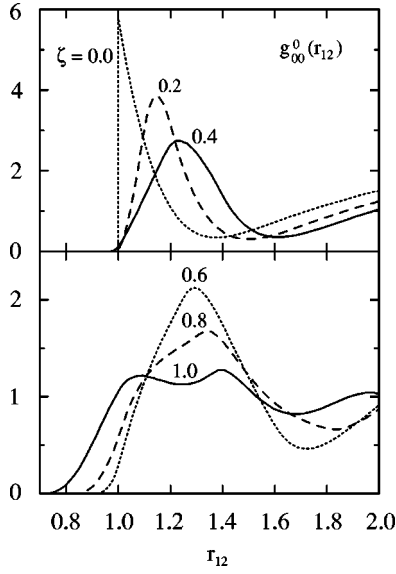
FIG. 6. Center-of-mass component of the molecular pair correlation function, $g_{00}^0(r_{12})$, as function of the center-to-center distance r_{12} at the fixed packing fraction $\varphi=0.56$ for various elongations ζ.

FIG. 7. The ϕ_{12}-averaged molecular pair correlation function $g(r_{12},\theta_1,\theta_2)$ as defined in Eq. (28) for the "T-shaped" ($\theta_1=0$, $\theta_2=\pi/2$) and the "CP-type" ($\theta_1=\theta_2=\pi/2$) orientations (see text) at the packing fraction $\varphi=0.56$ for the elongations $\zeta=0.4$ (upper panel) and 1.0 (lower panel).

elongations. On the other hand, when the elongation is large, the $\ell=2$ component is relevant, and this angular correlation becomes stronger with increasing elongation. This explains the increase of the first peak height in S_q^N with increasing ζ for large elongations. Thus, the nonmonotonic ζ dependence of the first peak height in S_q^N for the fixed packing fraction shown in Fig. 5 is due to the different origin of that peak for small and large elongations.

B. Preferred orientations for nearest neighbors

A digression might be adequate for a better understanding of the equilibrium structure of our molecular systems, especially, of angular correlations for nearest neighbors. Such angular correlations can best be investigated through the molecular pair correlation function $g(r_{12},\theta_1,\theta_2,\phi_{12})$. Here r_{12} denotes the center-to-center separation, and the three angles θ_1, θ_2, and $\phi_{12}\equiv\phi_1-\phi_2$ specify the relative orientations of the two linear molecules in the so-called r frame. The pair correlation function can be expanded as [35]

$$g(r_{12},\theta_1,\theta_2,\phi_{12})=4\pi\sum_{\ell_1,\ell_2,m}g_{\ell_1\ell_2}^m(r_{12})Y_{\ell_1}^m(\theta_1,\phi_1)$$
$$\times Y_{\ell_2}^m(\theta_2,\phi_2)^*. \quad (27)$$

The $g_{l_1l_2}^m(r_{12})$ are the spherical-harmonic expansion coefficients, and can be calculated within the PY theory [34,35]. In the present work, the coefficients are calculated up to cutoff $\ell_{cut}=6$.

The center-to-center radial-distribution functions $g_{00}^0(r_{12})$ for representative elongations at the large packing fraction $\varphi=0.56$ are shown in Fig. 6, along with the radial distribution function for hard spheres ($\zeta=0.0$) at the same packing fraction. As the elongation increases, the first peak position in $g_{00}^0(r_{12})$ increases, the height of the peak decreases, and
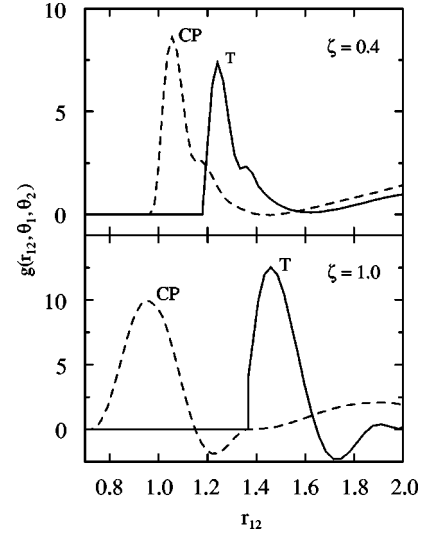
the peak becomes broader and somewhat irregular, with a shoulder developing at separations just beyond $r_{12}=1$. For the elongation $\zeta=1.0$, the shoulder turns into a broad prepeak centered at $r_{12}\approx1.1$.

It becomes more difficult to interpret the $g_{\ell_1\ell_2}^m(r_{12})$ for nonzero values of ℓ_1 and ℓ_2. Therefore it seems adequate to follow Streett and Tildesley [33] and consider cuts through the space of the four variables determining the function g in Eq. (27). Typical cuts for discussing the relative orientations of two linear molecules are [33] (i) the "T-shaped" orientation ($\theta_1=0$, $\theta_2=\pi/2$, $\phi_{12}=$ any value), (ii) the "crossed" orientation ($\theta_1=\theta_2=\phi_{12}=\pi/2$), (iii) the "parallel" orientation ($\theta_1=\theta_2=\pi/2$, $\phi_{12}=0$), and (iv) the "end-to-end" orientation ($\theta_1=\theta_2=0$, $\phi_{12}=$ any value). These orientations lead to efficient packing at close approach in the sense that they all lead to the close contact of the constituent atoms, and thus contribute to the first peak in S_q^N. Most of the orientations at high densities can be broadly classified as being similar to one of these four. Because of the computational reason to be described in the next paragraph, the crossed and parallel orientations shall be combined to define the CP-type orientation ($\theta_1=\theta_2=\pi/2$) by averaging over the angle ϕ_{12},

$$g(r_{12},\theta_1,\theta_2)\equiv\frac{1}{2\pi}\int_0^{2\pi}d\phi_{12}g(r_{12},\theta_1,\theta_2,\phi_{12}). \quad (28)$$

Notice that the corresponding ϕ_{12}-averaged pair correlation functions for the T-shaped ($\theta_1=0$, $\theta_2=\pi/2$) and end-to-end ($\theta_1=\theta_2=0$) orientations remain the same as the original ones since the angle ϕ_{12} is irrelevant in defining these two orientations. Figure 7 exhibits representative results.

Before embarking on the conclusions to be drawn from Figs. 6 and 7, let us make comments on the cutoff problem in the summation in Eq. (27). To check the convergence, we

also performed the same calculations with $\ell_{cut}=4$. It is found that for distances $r_{12}>1+\zeta$, the series converges rapidly, i.e., the difference between the results with $\ell_{cut}=4$ and those with $\ell_{cut}=6$ is small. However, for distances $r_{12}<1+\zeta$, the difference is rather large reflecting the slow convergence of the series, and this effect becomes more pronounced with increasing density and elongation. An indication of the lack of convergence is that the functions for $\zeta=1.0$ shown in the lower panel of Fig. 7 can take unphysical negative values in the range $r_{12}<1+\zeta$. The reason for the slow convergence in that range is that the function $g(r_{12},\theta_1,\theta_2,\phi_{12})$ has step-like features because of the hard-core repulsion, which cannot be accurately represented by a truncated series with a small value for ℓ_{cut}. This problem is likely to be a feature of the spherical-harmonic expansion for any model in which the molecule has a relatively hard asymmetric core. It is also found that a better convergence is achieved for the ϕ_{12}-averaged correlation function defined in Eq. (28) than the original $g(r_{12},\theta_1,\theta_2,\phi_{12})$, and this is why we have chosen the averaged ones to display the results. Despite these unwelcome features, it is anticipated that qualitative features of the angular correlations are captured even with $\ell_{cut}=6$. Notice that the mentioned cutoff problem does not influence the results to be presented for the MCT since those are based solely on S_q^N calculated from the RISM theory.

The increase of the most probable nearest neighbor center-to-center separation with increasing elongation, which is demonstrated in Fig. 6, suggests that the majority of nearest neighbor pairs adopt orientations for which the center-to-center distance of closest approach increases with increasing elongation. Therefore, it seems likely that "CP-type" orientations do not contribute heavily to this peak in $g_{00}^0(r_{12})$, because their closest approach remains in the region $r_{12}\approx1$ irrespective of the elongation. It is also clear that "end-to-end" orientations are unimportant, because their minimum approach distance ($r_{12}=1+\zeta$) lies well beyond the distance at which the first maximum occurs in $g_{00}^0(r_{12})$. Hence, the major contributions to the first peak in $g_{00}^0(r_{12})$ are likely to come from orientations of the T-shaped type and ones close to it. The first maximum in the $g(r_{12},\theta_1,\theta_2)$ for the T-shaped orientation for $\zeta=0.2$, 0.4, 0.6, 0.8, and 1.0 occur at $r_{12}=1.13$, 1.24, 1.33, 1.41, and 1.46, respectively, as shown in Fig. 7 for $\zeta=0.4$ and 1.0. These positions are very close to the first maximum positions in $g_{00}^0(r_{12})$ for each elongation shown in Fig. 6. This evidence is consistent with a strong predominance of T-shaped nearest neighbor orientations. We therefore conclude that at the most probable nearest neighbor distance, there is a strong preference for T-shaped orientations over all others.

We next consider how the CP-type correlations manifest themselves in the $g_{00}^0(r_{12})$. As can be inferred from Fig. 7, such correlations would lead to a peak centered at $r_{12}\approx1$ irrespective of the elongation. This contribution leads to a small shoulder as shown in Fig. 6 for $\zeta=0.6$. For the larger elongation $\zeta=0.8$, the shoulder gets more pronounced, and subsequently it leads to a broad peak at $r_{12}\approx1.1$ for $\zeta=1.0$.

Unlike hard spheres for which two centers cannot approach closer than $r_{12}=1$, two hard dumbbells can reach
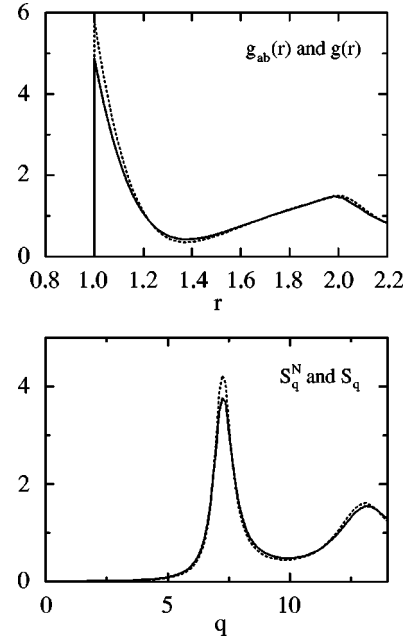

FIG. 8. Upper panel: the site-site radial-distribution function $g_{ab}(r)$ for the symmetric-hard-dumbbell system (see text) with $\zeta=1.0$ at the packing fraction $\varphi=0.56$ (solid line), and the radial-distribution function $g(r)$ for the hard-sphere system ($\zeta=0.0$) at the same packing fraction (dotted line). Lower panel: the corresponding static structure factor S_q^N for the total density fluctuations for the symmetric-hard-dumbbell system, and the static structure factor S_q for the hard-sphere system.

center-to-center distance $r_{12}<1$ by adopting a "crossed" orientation. This explains why the $g_{00}^0(r_{12})$ in Fig. 6 are positive even for $r_{12}<1$. The probability of the "crossed" orientation increases with increasing density because it relieves the strain of the closely packed system. This effect is more pronounced at high elongations as shown in Fig. 7, and is a major factor contributing to the growth of the shoulder in $g_{00}^0(r_{12})$ for the region $r_{12}<1$ with increasing the elongation.

Let us add one final comment. It is found from the extensions of the lower panel of Fig. 7 to the larger r_{12} region that both the T-shaped and CP-type correlations are rather long ranged. This is a manifestation of the strong peak in $S_{22}^0(q)$ at $q\approx0$ shown in Fig. 3 for $\zeta=1.0$, as was discussed also in Refs. [19] and [20]. The oscillatory feature of the above-mentioned angular correlations are found to continue up to $r_{12}\approx2\pi/\Delta q$, where Δq denotes the half-width of that peak in $S_{22}^0(q)$. This intermediate-range order is absent in the case of small elongations, say $\zeta=0.4$.

C. Bonding effects

The dumbbell liquid for $\zeta=1.0$ can be viewed as a system of hard spheres of diameter $d=1$ whose density is 2ρ and where some additional covalent interaction has forced pairs to be formed. Let us consider the difference between the hard-sphere system and the bonded system in detail. Figure 8 compares the the radial-distribution functions and the static structure factors for the two systems at the fixed packing fraction $\varphi=0.56$. Notice that the site-site radial-distribution

function $g_{ab}(r)$ for the symmetric-dumbbell system becomes independent of the site indices a and b, and this is the adequate quantity to be compared with the radial-distribution function $g(r)$ for the hard-sphere system. On the other hand, the total-density static structure factor S_q^N for the dumbbell system is the relevant one to be compared with the static structure factor S_q for the hard-sphere system. This is because, when the packing fraction is fixed, the number density for the hard dumbbells with $\zeta = 1.0$ is half of that for the hard spheres, and the function S_q^N properly accounts for this difference. The functions S_q^N and S_q are also the relevant inputs for the MCT equations for the hard-dumbbell and hard-sphere systems, respectively.

It is seen from the upper panel of Fig. 8 that the agreement of the radial-distribution functions for the two systems is very good except for the first-coordination-shell region. To demonstrate that this difference is primarily caused by the bonding, we shall consider the coordination number K, i.e., the number of nearest neighboring spheres surrounding a central sphere, which can be calculated from the radial-distribution function. It is found for the hard-sphere system that $K = 12.1$ at $\varphi = 0.56$, which is a typical value for simple systems at high density. So, K would tend to a value 12 also for the molecular system if the second sphere in one molecule was not attached to the first sphere. However, we found $K = 11.4$ for $\zeta = 1.0$ at $\varphi = 0.56$. Thus, as should be expected, the second sphere in one molecule excludes one sphere in another from being a nearest neighbor to the first sphere, and this results in the reduction of the radial-distribution function in the first-shell region as shown in the upper panel.

The observed feature for the radial-distribution functions also explains the reduction of the first peak height in the static structure factor for $\zeta = 1.0$ compared to that for $\zeta = 0.0$, as exhibited in the lower panel of Fig. 8. Let us consider what would happen to the static structure factor for the hard-sphere system when a short-ranged attractive force is added. This problem has been discussed for a square-well system [37]. As demonstrated there, the attraction causes bonding, in the sense that the most probable separation of two particles is smaller than expected for a pure hard-sphere system. This leads to the shift of the first peak position in the static structure factor to higher q, the decrease of the peak height, and the increase of the peak wings [37]. Although the first feature is not so prominent, the static structure factor for the $\zeta = 1.0$ dumbbell molecules reflects these features when compared to that for the hard-sphere system.

We conclude that the structure of the cage for the hard-dumbbell system with $\zeta = 1.0$ is very close to the one for the hard-sphere system, and that the difference can be explained as being due to the bonding effect.

IV. STRUCTURAL ARREST

A. Critical nonergodicity parameters

The upper panel of Fig. 9 exhibits the results for the nonergodicity parameters f_q^{Nc} at the critical point $\varphi = \varphi_c$ for the elongations $\zeta = 0.4$ and 1.0 calculated from Eq. (21). These are Debye-Waller factors of the system. They can be mea-
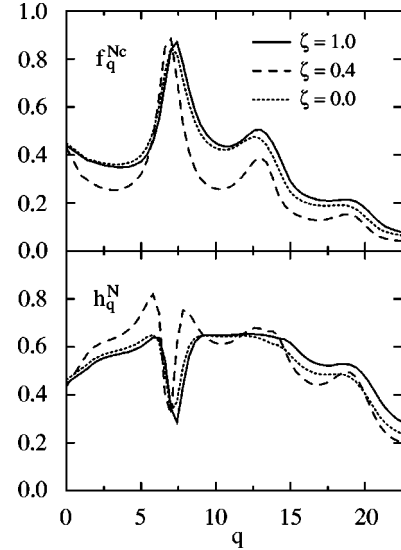

FIG. 9. Critical nonergodicity parameter f_q^{Nc} and critical amplitude h_q^N for the coherent total density fluctuations for the elongation $\zeta = 1.0$ (full lines), $\zeta = 0.4$ (dashed lines), and for the hard-sphere system ($\zeta = 0.0$, dotted lines).

sured, in principle, as cross section for coherent neutron scattering. For large S_q^N, the compressibility $\kappa_q \propto S_q^N$ is large. Therefore, spontaneous arrest is easier for larger S_q^N, and f_q^{Nc} exhibits a maximum near the first peak position of S_q^N. With varying q, f_q^{Nc} oscillates in phase with S_q^N (cf. Fig. 2). If the packing fraction increases, the arrested glass structure stiffens, i.e., the f_q^N increases. Expanding this increase for small distance parameters $\epsilon = (\varphi - \varphi_c)$, one finds [3,4]

$$f_q^N = f_q^{Nc} + D\sqrt{(\varphi - \varphi_c)}\, h_q^N + O(\varphi - \varphi_c). \tag{29}$$

The critical amplitude h_q^N is positive. It characterizes the susceptibility of the arrested structure with respect to changes of the control parameters. The formulas for the evaluation of h_q^N and of the constant $D > 0$ will be considered in the subsequent paper [26]. Since $f_q^N \leq 1$, $f_q^N - f_q^{Nc}$ is bounded by $1 - f_q^{Nc}$. Therefore, the critical amplitude h_q^N for the increase of f_q^N is much smaller for $q \approx 7$ than for q off the structure-factor-peak position, as shown in the lower panel of Fig. 9. These features are analogous to those found in the hard-sphere system [1,3].

Figure 10 exhibits the tagged-molecule's critical nonergodicity parameters $f_{q,s}^{xc}$ ($x = N$, Z) for the elongations $\zeta = 1.0$ and 0.4 calculated from Eq. (24). These are Lamb-Mössbauer factors describing the arrested probability distribution of the tagged molecule. As expected for a localized-distribution Fourier transform, the $f_{q,s}^{xc}$ versus q curves decrease with increasing q. The critical Lamb-Mössbauer factor $f_{q,s}^{Nc}$ for the total number density fluctuations approaches unity for q tending to zero due to the particle-number conservation law. On the other hand, there is no analogous conservation law for $x = Z$, and therefore one gets $f_{q \to 0,s}^{Zc} < 1$.
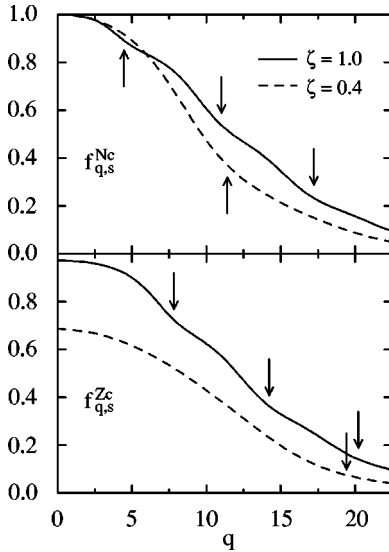
FIG. 10. Critical Lamb-Mössbauer factors for the tagged molecule's total density fluctuations $f_{q,s}^{Nc}$ (upper panel) and for the charge-density fluctuations $f_{q,s}^{Zc}$ (lower panel) for the elongation $\zeta = 1.0$ (full lines) and $\zeta = 0.4$ (dashed lines). The arrows indicate the wave numbers for the minimum positions in w_q^N and w_q^Z, respectively, calculated from Eq. (26).

A remarkable feature of Fig. 10 is the gentle oscillations exhibited by $f_{q,s}^{Nc}$ and $f_{q,s}^{Zc}$. In analogy to the discussion for f_q^{Nc}, it is expected that $f_{q,s}^{xc}$ oscillates in phase with w_q^x. As discussed in connection with Eq. (26), the function w_q^x exhibits minima because of various $j_\ell(q\zeta/2)^2$ contributions, and these minimum positions are marked as arrows in Fig. 10. One finds that the positions of the oscillations are well reproduced by the arrows, indicating that they are due to the presence of various angular-momentum-index ℓ contributions to intramolecular interference effects. A more definitive analysis concerning the origin of the oscillations should be based on the decomposition of $f_{q,s}^{xc}$ in terms of the nonergodicity parameters of the tensorial density correlators $\Phi_{s,\ell\ell'}^0(q,t)$ introduced in connection with Eq. (12) [24]. Under the diagonal approximation $\Phi_{s,\ell\ell'}^0(q,t) \approx \delta_{\ell\ell'}\Phi_{s,\ell\ell}^0(q,t)$, one gets from the long-time limit of Eq. (12),

$$f_{q,s}^{xc} = (2/w_q^x)\sum_\ell (2\ell+1)j_\ell(q\zeta/2)^2 f_s^c(q,\ell,0). \quad (30)$$

Here, $f_s^c(q,\ell,0) = \lim_{t\to\infty}\Phi_{s,\ell\ell}^0(q,t)$ for $\varphi = \varphi_c$, and ℓ should be even (odd) for $x = N(Z)$. As discussed in Ref. [24], the gentle oscillations exhibited by $f_{q,s}^{xc}$ can be explained as being due to the interference effects of $f_s^c(q,\ell,0)$ with the intramolecular form factors $j_\ell(q\zeta/2)^2$. Unfortunately, we do not have information on the $f_s^c(q,\ell,0)$.

It might be interesting to consider how the results for the total-density and charge-density fluctuations can be translated to those for the atomic density fluctuations. The latter can be obtained from the former via the inverse relation of Eqs. (16) and (17),
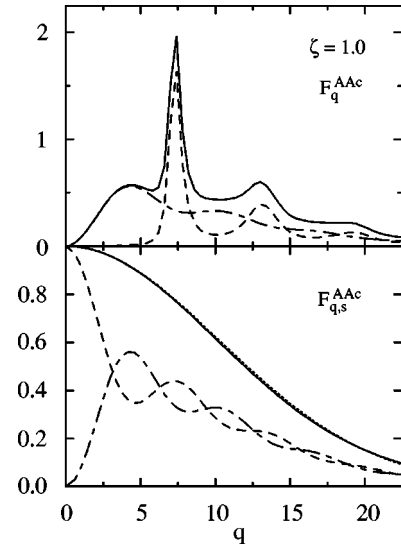

FIG. 11. The full lines exhibit the critical nonergodicity parameters for the atomic density fluctuations F_q^{AAc} (upper panel) and its self part $F_{q,s}^{AAc}$ (lower panel) for the elongation $\zeta = 1.0$. The dashed and dashed-dotted lines denote contributions from the total-density N and charge-density Z components, respectively. The dotted line in the lower panel denotes the result based on the Gaussian approximation for $F_{q,s}^{AAc}$, Eq. (32).

$$F_q^{AA} = \frac{1}{2}(f_q^N S_q^N + f_{q,s}^Z w_q^Z), \quad (31a)$$

$$F_{q,s}^{AA} = \frac{1}{2}(f_{q,s}^N w_q^N + f_{q,s}^Z w_q^Z). \quad (31b)$$

Notice that the self-part $F_{q,s}^{AA}$ can be measured as cross section for incoherent neutron scattering. The results at the critical packing fraction are exhibited as solid lines in Fig. 11 for the elongation $\zeta = 1.0$. The dashed and dashed-dotted lines are contributions from the total-density N and charge density fluctuations Z, respectively. A small peak centered at $q\approx4$ develops in F_q^{AAc} due to the charge-density fluctuations. The dotted line in the lower panel for the self-part $F_{q,s}^{AAc}$ denotes the result based on the Gaussian approximation

$$F_{q,s}^{AAc} \approx e^{-q^2(r_A^c)^2}. \quad (32)$$

Here, r_A^c is the critical localization length for atom A, defined via $\lim_{q\to0}(1-F_q^{AAc})/q^2 = (r_A^c)^2$. It is seen that the constituent atom's critical Lamb-Mössbauer factor $F_{q,s}^{AAc}$ is well described by a Gaussian, in particular, it does not exhibit oscillations. It is surprising that the sum of two non-Gaussian functions is almost Gaussian. The analogous results for $\zeta = 0.4$ are quite similar, except the peak of F_q^{AAc} for $q\approx4$ is suppressed.

B. Phase diagram

The phase diagram in Fig. 1 can be understood as a result of the control-parameter dependence of the structure factors which were explained in Sec. III. A prominent feature is the

maximum of the φ_c versus ζ curve near $\zeta = 0.43$. This is because of the two different mechanisms for the structural arrest, one dominating for small and the other one for large elongations. As discussed in connection with Fig. 2, the glass transition is driven by the first-peak region in the static structure factor S_q^N, irrespective of the elongation. For small elongations, the peak is primarily determined by the center-of-mass density fluctuations, and its strength becomes weaker with increasing elongation as explained in connection with Fig. 4 and the upper panel of Fig. 5. Therefore, a relatively higher packing fraction is required to get into the glassy phase if the elongation is increased, and this explains the increase of the $\varphi_c(\zeta)$ curve for small elongations. On the other hand, for large elongations, the first peak in S_q^N is mainly determined by the $\ell = 2$ angular correlation, and its magnitude gets larger with increasing the elongation as also explained in connection with Fig. 4 and the lower panel of Fig. 5. Thus, a relatively lower packing fraction is required for the glass formation as the elongation is increased, and this explains the decrease of the $\varphi_c(\zeta)$ curve for large elongations. As a result of these two competing mechanisms for the glass formation, the transition line $\varphi_c(\zeta)$ exhibits a maximum.

Another remarkable feature results from the structure-factor-peak reduction due to bonding, which was explained above in connection with Fig. 8. This reduction stabilizes the liquid phase. As a result, the critical packing fraction for elongation $\zeta = 1$, $\varphi_c(\zeta = 1) \approx 0.56$ is larger than that for the transition of the hard-sphere system, $\varphi_c(\zeta = 0) \approx 0.53$. Combined with the results discussed in the preceding paragraph, this implies that for all $0 < \zeta \leq 1$ the critical packing fraction of the hard-dumbbell system is larger than that of the hard-sphere system; the liquid phase gets expanded due to the formation of molecules. The increased-free-volume phenomenon due to the bond formation is consistent with the result discussed for a square-well system [37].

There are two alternatives for the glassy states, phases II and III in Fig. 1, with respect to the charge-density dynamics of the tagged molecule. Phase II deals with states for sufficiently small ζ. There is such small steric hindrance for a flip of the tagged molecule's axis between the two energetically equivalent positions $\vec{e}_s$ and $-\vec{e}_s$ that Eq. (24) for $x = Z$ yields $f_{q,s}^Z = 0$. The dynamics of the charge fluctuations is ergodic. In particular, the dipole correlator relaxes to zero: $C_{1,s}(t \to \infty) = 0$ where $C_{1,s}(t) = \langle \vec{e}_s(t) \cdot \vec{e}_s(0) \rangle = \phi_{q=0,s}^Z(t)$ [24]. For sufficiently large ζ, on the other hand, the steric hindrance for dipole reorientations becomes so effective, that also the charge fluctuations behave nonergodically. In this case, Eq. (24) for $x = Z$ yields a positive long time limit, $0 < f_{q,s}^Z = \phi_{q,s}^Z(t \to \infty)$. In particular, dipole disturbances do not relax to zero: $C_{1,s}(t \to \infty) = f_{1,s} = f_{q=0,s}^Z > 0$. This phase III is a glass with all structural disturbances exhibiting nonergodic motion. In particular, the nonergodicity parameter $f_{1,s}^c$ for, say, $\zeta \geq 0.6$ is as large as the maximum of f_q^{Nc}, Fig. 9. The two phases II and III are separated by a curve $\varphi_A(\zeta)$, where $\varphi_A(\zeta) \geq \varphi_c(\zeta)$. This curve is shown as the dashed line in Fig. 1. Since the steric hindrance for the molecule's flip motion increases with increasing ζ, one might expect that the curve
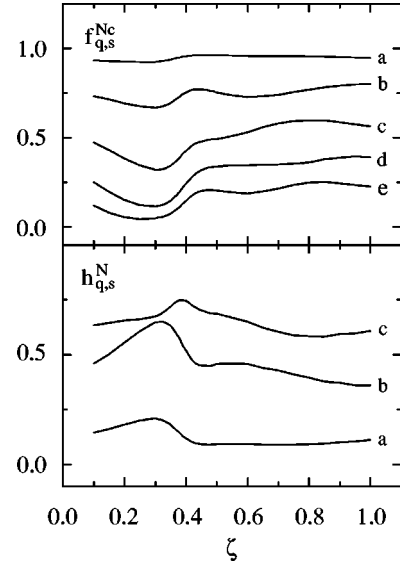

FIG. 12. Critical nonergodicity parameters $f_{q,s}^{Nc}$ and the critical amplitudes $h_{q,s}^N$ for the tagged molecule's total density fluctuations along the type-B transition line in Fig. 1 parametrized by the elongation ζ for the wave numbers $q = 3.4$ (a), 7.0 (b), 10.6 (c), 14.2 (d), and 17.4 (e). The critical amplitudes $h_{q,s}^N$ for $q = 14.2$ and 17.4 have been omitted to avoid the overlapping of the curves.

$\varphi_A(\zeta)$ would monotonically decrease with increasing ζ. However, this is not the case. What monotonically decreases with increasing ζ is the difference $\varphi_A(\zeta) - \varphi_c(\zeta)$, and the variation of $\varphi_c(\zeta)$ dominates that of $\varphi_A(\zeta)$ for small $\zeta_c - \zeta$. The curve $\varphi_A(\zeta)$ terminates at the critical elongation ζ_c: $\varphi_A(\zeta_c) = \varphi_c(\zeta_c)$. For our model, one finds $\zeta_c = 0.345$, and its position is marked by an arrow in Fig. 1. The asymptotic laws for the transition from phase II to phase III have earlier been described as the type-A transition, as can be inferred from Ref. [38] and the papers quoted there. The square-root singularity of the Debye-Waller factor f_q^N, Eq. (29), implies via Eq. (24) that the two phase-transition lines do not merge transversally: $(d/d\zeta)\varphi_A(\zeta_c) = (d/d\zeta)\varphi_c(\zeta_c)$. All together, this explains the minimum of the $\varphi_A(\zeta)$ versus ζ curve near $\zeta = 0.23$.

There are some characteristic features of the type-A transition that are relevant in the analysis of the type-B-transition dynamics: these are connected with the ζ variation of the critical Lamb-Mössbauer factors $f_{q,s}^{xc}$ and the critical amplitudes $h_{q,s}^x$ [26]. Figure 12 exhibits $f_{q,s}^{Nc}$ and $h_{q,s}^N$ for the total-density fluctuations along the type-B transition line $\varphi_c(\zeta)$ parametrized by ζ. Figure 13 shows the corresponding results for the charge-density correlator, $f_{q,s}^{Zc}$ and $h_{q,s}^Z$. They deal with the transition from phase II for $\zeta < \zeta_c$ to phase III for $\zeta > \zeta_c$. We note in passing that the curves shown in these figures exhibit nonmonotonic ζ dependence, such as wiggles, or even minima and maxima. These anomalies are analogs of the gentle oscillations, discussed above in connection with Fig. 10, and they can, in principle, be explained as was done in Ref. [24] for dumbbell molecules immersed in a hard-sphere system. For strong steric hindrance, say $\zeta \geq 0.8$, $f_{q,s}^{Nc}$ is rather close to $f_{q,s}^{Zc}$, and this holds also for critical ampli-
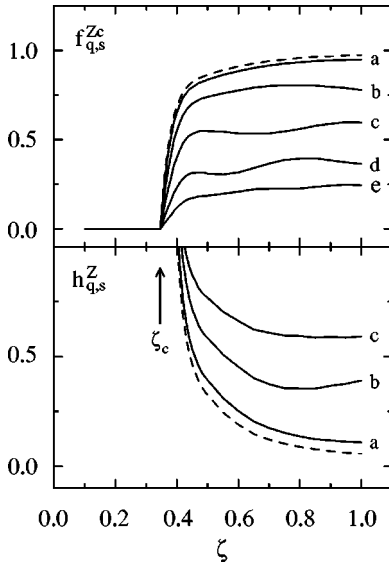
FIG. 13. Results as in Fig. 12, but for the tagged molecule's charge-density fluctuations, $f_{q,s}^{Zc}$ and $h_{q,s}^Z$. The dashed lines are added here, denoting the critical nonergodicity parameter (upper panel) and the critical amplitude (lower panel) for the zero-wave-number limit. The arrow marks the transition point from phase II to phase III at $\zeta_c = 0.345$ taken from Fig. 1.

tudes, $h_{q,s}^N$ and $h_{q,s}^Z$. For ζ approaching ζ_c, the Lamb-Mössbauer factor $f_{q,s}^{Zc}$ falls below $f_{q,s}^{Nc}$, and the critical amplitude $h_{q,s}^Z$ grows above $h_{q,s}^N$. These are characteristic features of the type-A transition, whose transition point can be characterized by the vanishing of the critical nonergodicity parameter $f_{q,s}^{Zc}$ and by the divergence of the critical amplitude $h_{q,s}^Z$ [38]. The former feature is demonstrated, for example, by the strong decrease of $f_{1,s}^c = f_{q \to 0,s}^{Zc}$ for $\zeta = 0.4$ shown in the lower panel of Fig. 10 compared to that for $\zeta = 1.0$ in the same panel. Since the critical amplitude $h_{q,s}^Z$ gauges the dynamics in the β-relaxation regime, the dynamics of the charge-density correlators as well as the dipole correlator near ζ_c is strongly influenced by precursor phenomena of the type-A transition from phase II to phase III. Their dynamics in the α-relaxation regime is also perturbed since the leading correction to the α-scaling law is proportional to the critical amplitude [3]. These features will be discussed in the following paper [26]. Thus, the dynamics for elongations close to ζ_c is qualitatively different from that for large elongations, and this is why we have chosen as the representative elongation $\zeta = 0.4$ for the demonstration of the state with weak steric hindrance for reorientations. Generically, there is no type-A transition line for arbitrary diatomic molecules. In our problem, this singularity is due to an additional symmetry that produces vanishing coupling constants. The top-down symmetry of the molecule renders the MCT equations to decouple completely into one set for total-density fluctuations and another one for charge-density fluctuations. For nearly top-down symmetrical molecules, the type-A transition is smeared to a rapid crossover from the very small nonergodicity parameters $f_{q,s}^Z$ for $\zeta \ll \zeta_c$ to those of order unity for $\zeta \gg \zeta_c$ [21,38,39]. By continuity, the critical

amplitude $h_{q,s}^Z$ remains large for ζ near ζ_c also for asymmetrical molecules. Therefore, the results for $\zeta = 0.4$ are also representative for such cases, where the type-A transition singularity is avoided due to breaking of the top-down symmetry of the constituent molecules, provided the breaking is sufficiently weak.

The described type-A transition has been studied also for a single dumbbell immersed in a system of hard spheres. The diagrams corresponding to the upper panels in Figs. 12 and 13 are qualitatively similar [39], but there are two remarkable differences. First, the form factors $f_{q,s}^{Nc}$ are somewhat larger and the variation with ζ for $\zeta \gtrsim \zeta_c$ is more pronounced for the hard-dumbbell system than for the corresponding quantities for the simple system. Similarly, for $\zeta > 0.5$ the $f_{q,s}^{Zc}$ are larger in Fig. 13 than for the single-dumbbell system. Second, the $(\zeta - \zeta_c)$ interval for the decay of $f_{q,s}^{Zc}$ from large weakly ζ-dependent values to zero at the transition is narrower for the motion in the dumbbell liquid than for the motion in the hard-sphere system. These differences reflect the fact that steric hindrance for translation as well as for reorientation is more efficient if the cage-forming neighbor molecules are sufficiently elongated rather than being spherical. This conclusion explains also that the obtained critical value $\zeta_c = 0.345$ is smaller than the corresponding value 0.380 obtained for a single dumbbell in a hard-sphere system [24].

V. CONCLUSIONS

A mode-coupling theory (MCT) for the evolution of glassy dynamics is derived and used to discuss the idealized liquid-glass transition in a hard-dumbbell system (HDS). The theory predicts a singular change of the dynamics caused by a regular change of the canonically defined equilibrium structure factors with variations of control parameters like the packing fraction φ. The structure factors define the mode-coupling constants in the equations of motion for the correlation functions, and they have been evaluated within the RISM and Percus-Yevick theories. The good agreement of the results from the two approximate approaches support the opinion that the used input information of the MCT is semiquantitatively correct. The results have been used to demonstrate that T-shaped configurations are the preferred arrangements of the cage-forming neighbors of a molecule. The observed arrangements are similar to those discussed earlier for more dilute systems [33]; but the ordering in our high-density regime is more pronounced. In addition, there is intermediate-ranged order leading to a central peak for quadrupole-density fluctuations, but this is irrelevant for the explanation of the glassy dynamics within the present theory (Sec. III). There is no information available on the correctness of the cited structure-factor theories within the large-φ regime studied in this paper. This implies obvious reservation concerning quantitative details of the results presented.

The MCT for molecular systems proposed in this paper is based on describing the dynamics by $(n \times n)$-matrix correlators formed with the n interaction-site densities of the molecule's constituent atoms. Such basis is inferior to that using a description by infinite-matrix correlators formed with

tensor-density fluctuations [14–22], provided the equations of motion of the latter theory could be solved for parameters and time regimes of interest. For example, our theory does not directly lead to results for the angular-momentum $\ell = 2$ reorientational correlator, which is relevant for the description of depolarized light-scattering data. However, it was shown already in some other context [24], how the $\ell = 2$ reorientational correlator can be obtained as an addendum of the site-representation theory. A more subtle extension of the theory would be necessary, if there exists second-order phase transition. A treatment of the interference of the slow glass dynamics with the critical dynamics of the phase transition would require the inclusion of the critical fluctuations in the relaxation kernel in the spirit of the original derivation of mode-coupling theories by Kawasaki [40]. It is unclear at present whether such an extension can be formulated.

Compared to a hard-sphere system (HSS), the fusion of two hard spheres to a dumbbell of elongation ζ, $0 < \zeta \leq 1$, increases the free volume if the packing fraction is kept fixed. Therefore, the liquid gets stabilized and the line for the liquid-to-glass transition $\varphi_c(\zeta)$ is above the transition value φ_c^{HSS} of the HSS. Like for the HSS, the transition is driven by the density fluctuations with wave vectors near the position of the first sharp diffraction peak. For small ζ, the peak is formed by the center-to-center correlations, which decrease with increasing ζ, leading to an increase of the φ_c versus ζ transition curve. For large ζ, the peak is formed by the quadrupole correlations; and these increase with ζ, leading to a decrease of the transition line. This explains the pronounced maximum of the transition curve in Fig. 1. The model studied exhibits a symmetry with respect to the top-down flip of the molecule's axis. As explained in the earlier MCT literature, this implies a line of spin-glass-type transitions shown as dashed curve in Fig. 1.

A comment concerning the accuracy of the reported calculations might be adequate. After the specified discretization of the wave numbers, Eq. (21) for the 100 numbers f_q^N is solved by the iteration $f_q^{N(j+1)} = \mathcal{F}_q^N[f^{N(j)}]/\{1 + \mathcal{F}_q^N[f^{N(j)}]\}$, $j = 0, 1, \ldots$, starting from $f_q^{N(0)} = 1$. The sequence decreases monotonically towards the nonergodicity parameter $f_q^{N(j)} \to f_q^N$. The linearized iteration for $\delta f_q^{(j)} = f_q^{N(j)} - f_q^N$ reads $\delta f_q^{(j+1)} = \Sigma_p A_{qp} \delta f_p^{(j)}$, where the Frobenius matrix $\mathbf{A}$ is given by $A_{qp} = (1 - f_q^N)^2 \partial \mathcal{F}_q^N[f^N]/\partial f_p^N$. The matrix has a maximum eigenvalue $E \leq 1$. Off the critical points, one gets $E < 1$, and the convergence of the iteration is exponentially fast. The critical point is characterized by $E^c = 1$, and here the convergence is only algebraically. The proofs of the cited mathematical properties can be found in Ref. [41]. Near the critical point, one derives from Eq. (29) $E^c - E \propto \sqrt{\varphi - \varphi_c}$. Analogous statements hold for the calculations of $f_{q,s}^Z$ from Eq. (24). In our numerical work, the value for E is controlled and $\varphi - \varphi_c$ is determined routinely so that $E^c - E \approx 10^{-4}$. Hence, the critical points are calculated with an accuracy of the order 10^{-8}. Thus, the accuracy of the lines in Fig. 1 is determined by the number n^* of values for ζ used to calculate $\varphi_c(\zeta)$ and $\varphi_A(\zeta)$. We used a grid with $n^* = 70$; it was chosen nonuniformly over the interval $0 \leq \zeta \leq 1$ with the

highest density of points for ζ near ζ_c.

Letz *et al.* have discussed a liquid-glass phase diagram for a system of hard ellipsoids [19]. Considering their aspect ratio of the prolate ellipsoids as an analog of $(\zeta + 1)$ for the dumbbells, their phase diagram looks similar to Fig. 1. They also show the analogue of the glass-to-glass transition curve, albeit without a minimum and with a transversal termination at the liquid-glass-transition line. It is argued in Ref. [19] that the strong decrease of the φ_c versus ζ curve for aspect ratios near 2 is an implication of the central peak of the angular-momentum $\ell = 2$ correlations, reflecting a nematic-transition precursor. Hence, the explanation of the phase diagram given in Ref. [19] for the hard-ellipsoid system is quite different from the explanation of Fig. 1 for the dumbbell system.

The critical form factors for the glass f_q^{Nc} quantify the arrested amorphous-density fluctuations at the transition. The wave-vector dependence, Fig. 9, is quite similar to that for a HSS. This reflects the fact that the cage around an interaction site is quite similar to that found for the HSS. The critical nonergodicity parameters $f_{q,s}^{Zc}$ for the arrest of the dipole reorientation, Fig. 13, are larger than the same quantities calculated for a single molecule in the HSS [24]. In particular, the decrease of $f_{q=0,s}^{Zc}$ for ζ decreasing to the critical value ζ_c is so abrupt, that the transition looks similar to a discontinuous one. This shows that steric hindrance for reorientation is more effective in a molecular system than in a system of spherical particles.

In a planned paper [26], it will be shown that the results for the arrested structure provide the key for an explanation of the structural relaxation.

ACKNOWLEDGMENTS

APPENDIX: MODE-COUPLING THEORY FOR MOLECULAR SYSTEMS

The MCT focuses on the dynamics of density fluctuations. Within the site representation, the basic variables are the density fluctuations for the n interaction sites of the N molecules: $\rho_q^a = \Sigma_{i=1}^N \exp(i\vec{q} \cdot \vec{r}_i^a)$, $a = 1, 2, \ldots, n$. Here $\vec{r}_i^a$ denotes the position vector of the site a in molecule i. The most important correlation functions for a statistical description of the dynamics are

$$F_q^{ab}(t) = \langle \rho_q^a(t)^* \rho_q^b(0) \rangle / N, \quad a, b = 1, \ldots, n. \quad (A1)$$

These n^2 functions shall be considered as the elements of an $n \times n$ matrix $\mathbf{F}_q(t)$. This matrix is real and symmetric. The short-time expansion of this matrix is given by

$$\mathbf{F}_q(t) = \mathbf{S}_q - \frac{1}{2} q^2 \mathbf{J}_q t^2 + O(t^4). \quad (A2)$$

Here the structure-factor matrix is given by $S_q^{ab} = \langle \rho_q^a(t)^* \rho_q^b(0) \rangle / N$, and $J_q^{ab} = \langle (\vec{q} \cdot \vec{j}_q^a)^* (\vec{q} \cdot \vec{j}_q^b) \rangle / Nq^2$ is defined in terms of the currents referring to the interaction sites

$\vec{j}_q^a = \sum_{i=1}^N \vec{v}_i^a \exp(i\vec{q}\cdot\vec{r}_i^a)$ with $\vec{v}_i^a$ denoting the velocity of the site a in molecule i. The Zwanzig-Mori formalism [28] leads to an exact equation of motion for $\mathbf{F}_q(t)$,

$$\partial_t^2 \mathbf{F}_q(t) + \mathbf{\Omega}_q^2 \mathbf{F}_q(t) + \mathbf{\Omega}_q^2 \int_0^t dt'\, \mathbf{m}_q(t-t')\partial_{t'}\mathbf{F}_q(t') = \mathbf{0},$$
$$(A3)$$

where

$$\mathbf{\Omega}_q^2 = q^2 \mathbf{J}_q \mathbf{S}_q^{-1}. \qquad (A4)$$

The right-hand side of this equation is a product of two positive definite matrices. Hence it is equivalent to the square of a positive definite matrix. Therefore, one can write it as the square, $\mathbf{\Omega}_q^2$, of some matrix $\mathbf{\Omega}_q$. Splitting off this matrix in front of the convolution integral is done for later convenience.

The difficult problem is the derivation of an approximation for the matrix $\mathbf{m}_q(t)$ of fluctuating-force correlations such that the cage effect is treated reasonably. This has been done originally in Ref. [23] by extending the procedure used for atomic systems [42]. But the reported formulas [23] are not acceptable. First, they do not properly reduce to those for simple systems in the united atom limit. Secondly, the momentum conservation law for coherent dynamics is not satisfied. For these reasons, an alternative derivation has been developed in Ref. [24] starting from the projection-operator theory of Mori and Fujisaka [43], albeit for molecules immersed in a simple system. It is possible to generalize this derivation for the coherent density correlators $\mathbf{F}_q(t)$ for molecular systems, but the procedure becomes more involved; it shall be described in a separate paper [44]. Here, a more simplified derivation shall be presented.

The simplified procedure starts by assuming that a molecular system is a mixture of constituent atoms; intramolecular constraints between constituent atoms are accounted for by the pair correlations only. In this way, a system of N molecules is treated as a mixture of n species, each consisting of N particles. Using the equations in MCT for mixtures [45], one gets the following expression for the relaxation kernel:

$$m_q^{ab}(t) = \mathcal{F}_q^{ab}[\mathbf{F}(t)], \qquad (A5)$$

where the mode-coupling functional $\mathcal{F}_q$ is given by the equilibrium quantities

$$\mathcal{F}_q^{ab}[\tilde{\mathbf{f}}] = \frac{1}{2}\sum_c S_q^{ac}\sum_{\lambda,\lambda',\mu,\mu'}\int d\vec{k}\, V_{\lambda\lambda'\mu\mu'}^{cb}(\vec{q};\vec{k},\vec{p})\tilde{f}_k^{\lambda\lambda'}\tilde{f}_p^{\mu\mu'},$$
$$(A6)$$

$$V_{\lambda\lambda'\mu\mu'}^{ab}(\vec{q};\vec{k},\vec{p}) = \frac{\rho}{(2\pi)^3}\{\vec{q}\cdot[\delta^{a\mu}\vec{k}c_k^{a\lambda} + \delta^{a\lambda}\vec{p}c_p^{a\mu}]\}$$

$$\times\{\vec{q}\cdot[\delta^{b\mu'}\vec{k}c_k^{b\lambda'} + \delta^{b\lambda'}\vec{p}c_p^{b\mu'}]\}/q^4,$$
$$(A7)$$

with $\vec{p} = \vec{q} - \vec{k}$. Here, the direct correlation function is defined via the Ornstein-Zernike equation for a mixture [28], $\rho c_q^{ab} = \delta^{ab} - (S_q^{-1})^{ab}$. Now, let us turn on the intramolecular constraints between constituent atoms. This amounts to replacing the direct correlation function c_q^{ab} for a mixture of spherical particles with that for molecular systems defined via the site-site Ornstein-Zernike equation [27,28], $\rho c_q^{ab} = (w_q^{-1})^{ab} - (S_q^{-1})^{ab}$. Here enter the intramolecular correlation functions w_q^{ab} describing the constraints. The so obtained equations for a mixture contain a frequency matrix $\mathbf{\Omega}_q^2$, which reflects the $3n$ independent degrees of freedom of the molecule. In particular, $\mathbf{\Omega}_q^2$ gets an n-fold degenerate eigenvalue zero for $q=0$ due to the n particle-number-conservation laws for the n species. The used classical theory cannot account for the fact that vibrational degrees of freedom are frozen out at sufficiently low temperature because of quantum effects. To repair this shortcoming, we make the assumption that in the regime of interest the rigidity of the molecule can be accounted for by replacing the classical flexible-molecule value for $\mathbf{\Omega}_q^2$ in front of the convolution integral in Eq. (A3) by the formula in Eq. (A4). The matrix $\mathbf{\Omega}_q^2$ for a rigid molecule exhibits only one eigenvalue zero for $q=0$, since there is only one independent conservation law for the number of molecules.

The MCT equations for the tagged-molecule density correlator $\mathbf{F}_{q,s}(t)$ defined in Eq. (5) can be obtained similarly, and only the resulting equations shall be quoted. The exact Zwanzig-Mori equation reads

$$\partial_t^2 \mathbf{F}_{q,s}(t) + \mathbf{\Omega}_{q,s}^2 \mathbf{F}_{q,s}(t) + \mathbf{\Omega}_{q,s}^2\int_0^t dt'\, \mathbf{m}_{q,s}(t-t')$$

$$\times\partial_{t'}\mathbf{F}_{q,s}(t') = \mathbf{0}, \qquad (A8)$$

where the characteristic frequency matrix is given as in Eq. (A4) by $\mathbf{\Omega}_{q,s}^2 = q^2 \mathbf{J}_q \mathbf{w}_q^{-1}$. The expression for the relaxation kernel can be formulated as the mode-coupling functional $\mathcal{F}_{q,s}$,

$$m_{q,s}^{ab}(t) = \mathcal{F}_{q,s}^{ab}[\mathbf{F}_s(t),\mathbf{F}(t)]. \qquad (A9)$$

The explicit expression for the functional $\mathcal{F}_{q,s}$ reads, with $\vec{p} = \vec{q} - \vec{k}$,

$$\mathcal{F}_{q,s}^{ab}[\tilde{f}_s,\tilde{f}] = \frac{\rho}{(2\pi)^3}\sum_c \frac{w_q^{ac}}{q^2}\sum_{\lambda,\mu}\int d\vec{k}$$

$$\times\left(\frac{\vec{q}\cdot\vec{p}}{q}\right)^2 c_p^{c\lambda}c_p^{b\mu}\tilde{f}_{k,s}^{cb}\tilde{f}_p^{\lambda\mu}. \qquad (A10)$$

Let us note some mathematical results valid for the MCT formulated above. First of all, there is a solution $\mathbf{F}_q(t)$ of the nonlinear equations of motion for all times t. This solution is uniquely fixed by the initial conditions $\mathbf{F}_q(t=0) = \mathbf{S}_q$ and $\partial_t\mathbf{F}_q(t=0) = \mathbf{0}$. For every finite time interval, the solution depends smoothly on the numbers Ω_q^{2ab} and

$V^{ab}_{\lambda\lambda'\mu\mu'}(\vec{q};\vec{k},\vec{p})$. The solutions are correlation functions in the sense that they can be Laplace transformed to functions having a spectral representation with a spectrum $\mathbf{F}''_q(\omega)$, which is a positive definite matrix. The matrix of long time limits, $\mathbf{F}_q = \lim_{t\to\infty}\mathbf{F}_q(t)$, obeys the set of implicit equations defined by the mode-coupling functional $\mathcal{F}_q$,

$$\mathbf{F}_q[\mathbf{S}_q - \mathbf{F}_q]^{-1} = \mathcal{F}_q[\mathbf{F}]. \tag{A11}$$

Let us remember that there is a semiordering in the space of real symmetric $n\times n$ matrices, $\mathbf{A} > \mathbf{B}$, defined by $\mathbf{A} - \mathbf{B}$ to be positive definite. With this notation, the maximum theorem holds: if $\hat{\mathbf{F}}_q$ is a solution of Eq. (A11), i.e., if $\hat{\mathbf{F}}_q[\mathbf{S}_q - \hat{\mathbf{F}}_q]^{-1} = \mathcal{F}_q[\hat{\mathbf{F}}]$, then $\hat{\mathbf{F}}_q \leqslant \mathbf{F}_q$. If an iteration sequence $\mathbf{F}_q^{(j)}$, $j = 0, 1, \dots$, is defined by $\mathbf{F}_q^{(j+1)}[\mathbf{S}_q - \mathbf{F}_q^{(j+1)}]^{-1} = \mathcal{F}_q[\mathbf{F}^{(j)}]$ starting from $\mathbf{F}_q^{(0)} = \mathbf{S}_q$, then $\mathbf{F}_q^{(j+1)} < \mathbf{F}_q^{(j)}$ and

$\lim_{j\to\infty}\mathbf{F}_q^{(j)} = \mathbf{F}_q$. If the Jacobian of Eq. (A11) does not have a vanishing eigenvalue, the long-time limit $\mathbf{F}_q$ depends smoothly on the coupling coefficients $V^{ab}_{\lambda\lambda'\mu\mu'}(\vec{q};\vec{k},\vec{p})$. A singularity can occur only if an eigenvalue vanishes. The subtlest property is that such a vanishing eigenvalue is non-degenerate. Hence, using the terminology of Arnold [46], all possible singularities are bifurcations of the cuspoid type A_ℓ, $\ell = 2, 3, \dots$. The generic singularity for changes of a single control parameter is, as for the MCT of simple systems, a fold bifurcation A_2. It is then obvious that all universal results for simple systems are valid also for the MCT for molecular systems formulated above. For example, Eq. (29) holds with f_q^{Nc} and h_q^N replaced by positive definite matrices. The proofs of the cited results of this paragraph shall not be described here for brevity, since essentially the same issues for matrices of density correlators have been independently discussed and proved by Franosch and Voigtmann [47].

---

[1] U. Bengtzelius, W. Götze, and A. Sjölander, J. Phys. C **17**, 5915 (1984).

[2] S. F. Edwards and P. W. Anderson, J. Phys. F: Met. Phys. **5**, 965 (1975).

[3] T. Franosch, M. Fuchs, W. Götze, M. R. Mayr, and A. P. Singh, Phys. Rev. E **55**, 7153 (1997), and references therein.

[4] M. Fuchs, W. Götze, and M. R. Mayr, Phys. Rev. E **58**, 3384 (1998).

[5] W. Götze and L. Sjögren, Rep. Prog. Phys. **55**, 241 (1992).

[6] W. Götze, J. Phys.: Condens. Matter **11**, A1 (1999).

[7] W. Kob, J. Phys.: Condens. Matter **11**, R85 (1999).

[8] R. Torre, P. Bartolini, M. Ricci, and R. M. Pick, Europhys. Lett. **52**, 324 (2000).

[9] G. Hinze, D. D. Brace, S. D. Gottke, and M. D. Fayer, Phys. Rev. Lett. **84**, 2437 (2000).

[10] J. Wiedersich, N. V. Surovtsev, and E. Rössler, J. Chem. Phys. **113**, 1143 (2000).

[11] F. Sciortino and W. Kob, Phys. Rev. Lett. **86**, 648 (2001).

[12] C. Bennemann, J. Baschnagel, and W. Paul, Eur. Phys. J. B **10**, 323 (1999).

[13] F. Sciortino and P. Tartaglia, J. Phys.: Condens. Matter **11**, A261 (1999).

[14] R. Schilling and T. Scheidsteger, Phys. Rev. E **56**, 2932 (1997).

[15] C. Theis and R. Schilling, J. Non-Cryst. Solids **235-237**, 106 (1998).

[16] L. Fabbian, A. Latz, R. Schilling, F. Sciortino, P. Tartaglia, and C. Theis, Phys. Rev. E **60**, 5768 (1999).

[17] A. Winkler, A. Latz, R. Schilling, and C. Theis, Phys. Rev. E **62**, 8004 (2000).

[18] C. Theis, F. Sciortino, A. Latz, R. Schilling, and P. Tartaglia, Phys. Rev. E **62**, 1856 (2000).

[19] M. Letz, R. Schilling, and A. Latz, Phys. Rev. E **62**, 5173 (2000).

[20] T. Theenhaus, R. Schilling, A. Latz, and M. Letz, Phys. Rev. E **64**, 051505 (2001).

[21] T. Franosch, M. Fuchs, W. Götze, M. R. Mayr, and A. P. Singh, Phys. Rev. E **56**, 5659 (1997).

[22] W. Götze, A. P. Singh, and Th. Voigtmann, Phys. Rev. E **61**, 6934 (2000).

[23] S.-H. Chong and F. Hirata, Phys. Rev. E **58**, 6188 (1998).

[24] S.-H. Chong, W. Götze, and A. P. Singh, Phys. Rev. E **63**, 011 206 (2001).

[25] S.-H. Chong, W. Götze, and M. R. Mayr, Phys. Rev. E **64**, 011 503 (2001).

[26] S.-H. Chong and W. Götze (unpublished).

[27] D. Chandler and H. C. Andersen, J. Chem. Phys. **57**, 1930 (1972).

[28] J.-P. Hansen and I. R. McDonald, *Theory of Simple Liquids*, 2nd ed. (Academic Press, London, 1986).

[29] S.-H. Chong and F. Hirata, Phys. Rev. E **57**, 1691 (1998).

[30] L. J. Lowden and D. Chandler, J. Chem. Phys. **59**, 6587 (1973).

[31] P. J. Rossky and H. L. Friedman, J. Chem. Phys. **72**, 5694 (1980).

[32] W. H. Press, S. A. Teukolsky, W. T. Vetterling, and B. P. Flannery, *Numerical Recipes in C: The Art of Scientific Computing*, 2nd ed. (Cambridge University Press, Cambridge, 1993).

[33] W. B. Streett and D. J. Tildesley, Proc. R. Soc. London, Ser. A **348**, 485 (1976).

[34] Y.-D. Chen and W. A. Steele, J. Chem. Phys. **54**, 703 (1971).

[35] C. G. Gray and K. E. Gubbins, *Theory of Molecular Fluids* (Clarendon Press, Oxford, 1984), Vol. 1.

[36] M. Letz and A. Latz, Phys. Rev. E **60**, 5865 (1999).

[37] K. Dawson, G. Foffi, M. Fuchs, W. Götze, F. Sciortino, M. Sperl, P. Tartaglia, Th. Voigtmann, and E. Zaccarelli, Phys. Rev. E **63**, 011401 (2000).

[38] T. Franosch and W. Götze, J. Phys.: Condens. Matter **6**, 4807 (1994).

[39] T. Franosch and A. P. Singh, J. Non-Cryst. Solids **235-237**, 153 (1998).

[40] K. Kawasaki, Phys. Rev. **150**, 291 (1966).

[41] W. Götze and L. Sjögren, J. Math. Anal. Appl. **195**, 230 (1995).

[42] W. Götze, in *Liquids, Freezing and Glass Transition*, edited by J.-P. Hansen, D. Levesque, and J. Zinn-Justin (North-Holland, Amsterdam, 1991), p. 287.

[43] H. Mori and H. Fujisaka, Prog. Theor. Phys. **49**, 764 (1973).

[44] S.-H. Chong (unpublished).

[45] J.-L. Barrat and A. Latz, J. Phys.: Condens. Matter **2**, 4289 (1990).

[46] V. I. Arnold, *Catastrophe Theory*, 3rd ed. (Springer-Verlag, Berlin, 1992).

[47] T. Franosch and Th. Voigtmann (unpublished).